Article

On the Electronic Origins of Structural Isomerism in the Iron–Sulfur Cubane, [(CH)FeS]

Sushilla Z. Knottenbelt, and John E. McGrady

J. Am. Chem. Soc., **2003**, 125 (32), 9846-9852• DOI: 10.1021/ja0353053 • Publication Date (Web): 19 July 2003

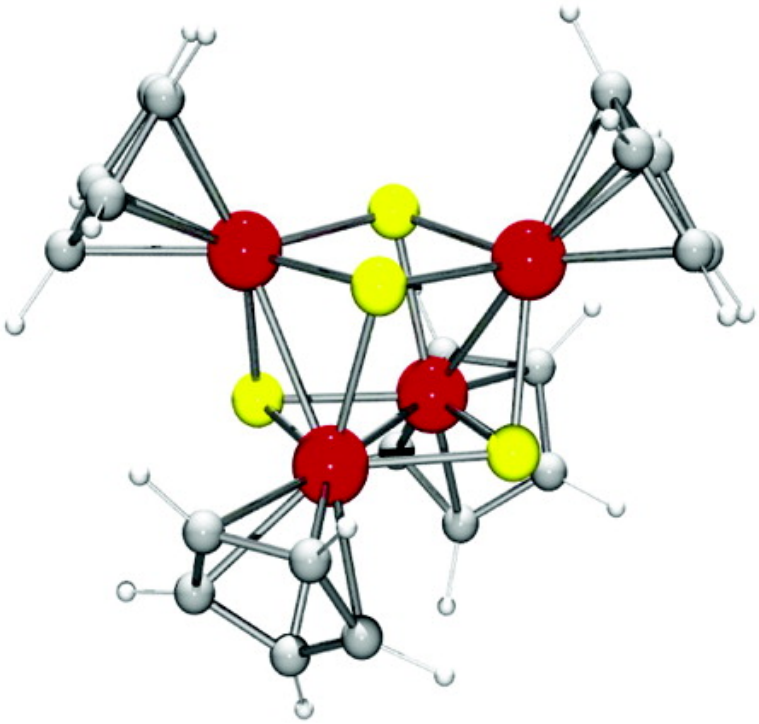

J|A|C|S
ARTICLES
Published on Web 07/19/2003

On the Electronic Origins of Structural Isomerism in the Iron−Sulfur Cubane, $[(C_5H_5)_4Fe_4S_4]^{2+}$

Sushilla Z. Knottenbelt and John E. McGrady*

Contribution from the Department of Chemistry, The University of York, Heslington, York, YO10 5DD, United Kingdom

Received March 25, 2003; E-mail: jem15@york.ac.uk

Abstract: Density functional theory provides new insights into the structural isomerism observed in the cyclopentadienyl-capped iron−sulfur cluster, $[(C_5H_5)_4Fe_4S_4]^{2+}$. Two distinct, closely spaced minima have been located, a triplet with D_2 symmetry and a C_2-symmetric singlet, both of which correspond closely to the structure of one of the known crystal forms of the cation. Thus, the structural diversity in these species reflects genuine molecular bistability rather than simple solid-state packing effects. In contrast, no stable D_{2d}-symmetric minimum has been located, suggesting that the reported D_{2d} symmetry of the cation in $[(C_5H_5)_4Fe_4S_4][PF_6]_2$ may be a crystallographic artifact. In the ruthenium analogue, the more diffuse 4d orbitals stabilize the C_2-symmetric singlet, which is unambiguously the ground state, but the D_2-symmetric potential energy surface provides a viable low-energy pathway for the dynamic exchange of the Ru−Ru bonds.

Introduction

The electronic structure of iron−sulfur clusters continues to attract a great deal of attention in the literature, largely in the context of biological electron transfer processes.[1−6] Even before their biological role was fully appreciated, however, the intrinsic appeal of highly symmetric clusters of metal ions had inspired a number of researchers to synthesize and study a wide range of metal cubanes. Perhaps the most ubiquitous of these are the cyclopentadienyl-capped species, $(C_5H_5)_4M_4E_4$ (E = O,S) (Chart 1), which are known for the majority of the transition metals.[7−22]

The available crystallographic data, collected in Table 1, show that the metal core is almost perfectly tetrahedral in some cases

Chart 1. Structure of a Cyclopentadienyl-Capped Cubane Cluster

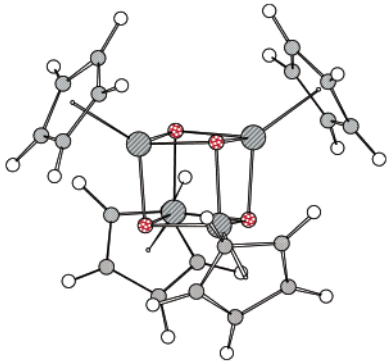

but highly distorted in others, and this structural diversity encouraged Dahl and co-workers to conduct the first investiga-

(1) (a) Hagen, W. R. *Adv. Inorg. Chem.* **1992**, *38*, 165. (b) Bertini, I.; Ciurli, S.; Luchinat, C. *Struct. Bonding* **1995**, *83*, 1.
(2) (a) Yoo, S. J.; Angove, H. C.; Burgess, B. K.; Münck, E.; Peterson, J. *J. Am. Chem. Soc.* **1998**, *120*, 9704. (b) Yoo, S. J.; Angove, H. C.; Burgess, B. K.; Hendrich, M. P.; Münck, E. *J. Am. Chem. Soc.* **1999**, *121*, 2534. (c) Sanakis, Y.; Yoo, S. J.; Osterloh, F.; Holm, R. H.; Münck, E. *Inorg. Chem.* **2002**, *41*, 7081. (d) Sanakis, Y.; Macedo, A. L.; Moura, I.; Moura, J. J. G.; Papaefthymiou, V.; Munck, E. *J. Am. Chem. Soc.* **2000**, *122*, 11855.
(3) (a) Rose, K.; Shadle, S. E.; Glaser, T.; de Vries, S.; Cherepanow, A.; Canters, G. W.; Hedman, B.; Hodgson, K. O.; Solomon, E. I. *J. Am. Chem. Soc.* **1999**, *121*, 2353. (b) Glaser, T.; Hedman, B.; Hodgson, K. O.; Solomon, E. I. *Acc. Chem. Res.* **2000**, *33*, 859.
(4) (a) Noodleman, L.; Case, D. A. *Adv. Inorg. Chem.* **1992**, *38*, 423. (b) Aizman A.; Case, D. A. *J. Am. Chem. Soc.* **1982**, *104*, 3269. (c) Noodleman, L.; Peng, C. Y.; Case, D. A.; Mouesca, J.-M. *Coord. Chem. Rev.* **1995**, *144*, 199. Lovell, T.; Torres, R. A.; Han, W.-G.; Liu, T.; Case, D. A.; Noodleman, L. *Inorg. Chem.* **2002**, *41*, 5744. Lovell, T.; Li, J.; Liu, T.; Case, D. A.; Noodleman, L. *J. Am. Chem. Soc.* **2001**, *123*, 12392. Torres, R. A.; Lovell, T.; Noodleman, L.; Case, D. A. *J. Am. Chem. Soc.* **2003**, *125*, 1923.
(5) Sigfridsson, E.; Olsson, M. H. M.; Ryde, U. *Inorg. Chem.* **2001**, *40*, 2509.
(6) (a) Szilagyi, R. K.; Musaev, D. G.; Morokuma, K. *Inorg. Chem.* **2001**, *40*, 766. (b) Datta, S. N.; Nehra, V.; Jha, A. *J. Phys. Chem. B* **1999**, *103*, 8768. (c) Thomson, A. J. *J. Chem. Soc., Dalton Trans.* **1981**, 1180.
(7) Darkwa, J.; Lockemeyer, J. R.; Boyd, P. D. W.; Rauchfuss, T. B.; Rheingold, A. L. *J. Am. Chem. Soc.* **1988**, *110*, 141.
(8) Bandy, J. A.; Davies, C. E.; Green, J. C.; Green, M. L. H.; Prout, K.; Rodgers, D. P. S. *J. Chem. Soc., Chem. Commun.* **1983**, 1395.
(9) Eremenko, I. L.; Nefedov, S. E.; Pasynskii, A. A.; Orazsakhatov, B.; Ellert, O. G.; Struchkov, Yu. T.; Yanovsky A. I.; Zagorevsky, D. V. *J. Organomet. Chem.* **1989**, *368*, 185.
(10) (a) Bottomley, F.; Paez, D. E.; White, P. S. *J. Am. Chem. Soc.* **1981**, *103*, 5581. (b) Bottomley, F.; Paez, D. E.; White, P. S. *J. Am. Chem. Soc.* **1982**, *104*, 5651. (c) Bottomley, F.; Paez, D. E.; Sutin, L.; White, P. S.; Köhler, F. H.; Thompson R. C.; Westwood, N. P. C. *Organometallics* **1990**, *9*, 2443.
(11) Bottomley, F.; Chen, J.; MacIntosh, S. M.; Thompson, R. C. *Organometallics* **1991**, *10*, 906.
(12) Wei, C.; Goh, L.-Y. Bryan, R. F.; Sinn, E. *Acta Crystallogr., Sect. C* **1986**, *42*, 796.
(13) Pasynskii, A. A.; Eremenko, I. L.; Rakitin, Yu. V.; Novotortsev, V. M.; Ellert, O. G.; Kalinnikov, V. T.; Shklover, V. E.; Struchkov, Yu. T.; Lindeman, S. V.; Kurbanov, T. Kh.; Gasanov, G. Sh. *J. Organomet. Chem.* **1983**, *248*, 309.
(14) Trinh-Toan; Teo, B. K.; Ferguson, J. A.; Meyer, T. J.; Dahl, L. F. *J. Am. Chem. Soc.* **1977**, *99*, 408.
(15) Bellamy, D.; Christofides, A.; Connelly, N. G.; Lewis, G. R.; Orpen, A. G.; Thornton, P. *J. Chem. Soc., Dalton Trans.* **2000**, 4038.
(16) (a) Houser, E. J.; Amarasekera, J.; Rauchfuss, T. B.; Wilson, S. R. *J. Am. Chem. Soc.* **1991**, *113*, 7440 (b) Houser, E. J.; Rauchfuss, T. B.; Wilson, S. R. *Inorg. Chem.* **1993**, *32*, 4069.
(17) Trinh-Toan; Fehlhammer, W. P.; Dahl, L. F. *J. Am. Chem. Soc.* **1977**, *99*, 402.
(18) (a) Schunn, R. A.; Fritchie, C. J.; Prewitt, C. T. *Inorg. Chem.* **1966**, *5*, 892. (b) Wei, C. H.; Wilkes, G. R.; Treichel, P. M.; Dahl, L. F. *Inorg. Chem.* **1966**, *5*, 900.

10.1021/ja0353053 CCC: $25.00

Table 1. Structures of Metal Cubanes, $(C_5R_5)_4M_4E_4$

complex	cluster electron count	(M–M)/Å	ref	complex	cluster electron count	(M–M)/Å	ref
$(C_5Me_5)_4Ti_4S_4$	4	2.93 × 2, 3.01× 4	7	$[(C_5H_5)_4Fe_4S_4]^{2+}[PF_6]_2$	18	2.83 × 4, 3.25 × 2	14
$(C_5H_4Me)_4V_4S_4^+$	7	2.85−2.86	7	$[(C_5H_5)_4Fe_4S_4]^{2+}[Ni(mnt)_2]$	18	2.66 × 2, 2.97 × 2, 3.27 × 2	15
$(C_5H_4Me)_4V_4S_4$	8	2.87−2.88	7	$[(C_5H_5)_4Fe_4S_4]^{2+}[Pt(mnt)_2]_2$	18	2.65 × 2, 3.27 × 3	15
$(C_5H_4{}^iPr)_4Mo_4S_4^{2+}$	10	2.81 × 2, 2.89 × 4	8	$[(C_5H_5)_4Fe_4S_4]^{2+}[Pt(mnt)_2]_2$	18	2.65 × 2, 2.90, 3.08, 3.26 × 2	15
$(C_5H_4{}^iPr)_4Mo_4S_4^+$	11	2.83−2.84	8	$(C_5H_4Me)_4Ru_4S_4^{2+}$	18	2.79, 2.78 × 2, 3.47 × 2, 3.56	16
$(C_5H_4Me)_4Cr_4O_4$	12	2.90 × 2, 2.76 × 4	9	$(C_5H_5)_4Fe_4S_4^+$	19	2.57 × 2, 3.19 × 2, 3.32 × 2	17
$(C_5H_5)_4Cr_4O_4$	12	2.90 × 2, 2.82 × 2, 2.71 × 2	10	$(C_5H_5)_4Fe_4S_4$	20	2.65 × 2, 3.36 × 4	18
$(C_5Me_5)_4Cr_4O_4$	12	2.83−2.84	11	$(C_5H_4Me)_4Ru_4S_4$	20	2.75 × 2, 3.60 × 4	19
$(C_5H_5)_4Cr_4S_4$	12	2.82−2.89	12	$(C_5Me_5)_4Ir_4S_4^{2+}$	22	2.76, 3.57 × 4, 3.68	20
$(C_5H_4Me)_4Cr_4S_4$	12	2.82−2.85	13	$(C_5H_5)_4Co_4S_4^+$	23	3.33 × 2, 3.17 × 4	21
$(C_5H_4{}^iPr)_4Mo_4S_4$	12	2.89−2.91	8	$(C_5Me_5)_4Ir_4S_4$	24	3.58−3.60	22
				$(C_5H_5)_4Co_4S_4$	24	3.22−3.34	21

Scheme 1. Dahl Model of Electronic Structure for Metal Cubanes

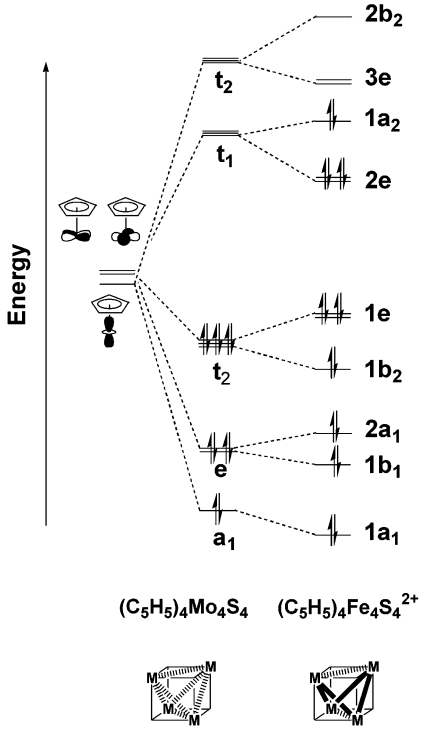

tions into their electronic structure.[14,23] The Dahl model is based on the concept that each metal center contributes three orbitals (the t_{2g} set of an idealized octahedron) to the bonding manifold. These twelve orbitals split, in perfect tetrahedral symmetry, into metal−metal bonding ($a_1 + e + t_2$) and antibonding ($t_1 + t_2$) subsets (Scheme 1). Occupation of all six bonding orbitals gives a bond order of 1 for each edge of the tetrahedron and, hence, leads to a symmetric tetrahedral geometry with short M−M separations, as is observed in $(C_5H_4{}^iPr)_4Mo_4S_4$. The addition of 12 further electrons fills the antibonding manifold, also resulting in a tetrahedral structure, but this time with no net metal−metal bonding, as in $(C_5H_5)_4Co_4S_4$. Between these two extremes, partial occupation of the antibonding manifold leads to highly distorted structures, as exemplified by the series $[(C_5H_5)_4Fe_4S_4]^{2+/1+/0}$ (18, 19, and 20 cluster electrons, respectively). The neutral species adopts a D_{2d}-symmetric structure with two short Fe−Fe bonds (Table 1), consistent with the presence of eight electrons in the antibonding manifold, leading to the cleavage of the bonds along four of the six edges of the tetrahedron. By analogy, the six antibonding electrons in the dication should break three of the Fe−Fe bonds, and so the presence of *four* equivalent short Fe−Fe bonds in $[(C_5H_5)_4Fe_4S_4][PF_6]_2$ was unexpected. The Dahl model, however, provided a resolution to this apparent anomally by showing that the vacant orbital of b_2 symmetry is antibonding with respect to all four short Fe−Fe contacts, each of which therefore has a bond order of $^3/_4$ rather than 1.

Since the original publications in the 1970s,[14,23] several groups have proposed modifications to the Dahl model,[24] most notably where anomalies occur due to very weak orbital overlap.[11,25] In the context of the iron−sulfur cubanes, however, the original model of electronic structure has remained largely unchallenged. A number of recent experimental observations, however, suggest that the situation may be rather more complex than previously suspected. The isoelectronic ruthenium species, $[(C_5H_5)_4Ru_4S_4]^{0/2+}$, synthesized by Rauchfuss and co-workers,[16,19] offer an illuminating comparison with their iron analogues. The neutral species is very similar to its iron congener, with two short Ru−Ru bonds in a D_{2d}-symmetric structure. In contrast, the C_2-symmetric structure of the ruthenium dication, with three distinct short Ru−Ru bonds, is very different from the dication in $[(C_5H_5)_4Fe_4S_4][PF_6]_2$ but more consistent with the 18 cluster-electron count. The story was further complicated by a recent report from Orpen and co-workers, where the $[(C_5H_5)_4Fe_4S_4]^{2+}$ cation was crystallized with two additional counterions, $[Ni(mnt)_2]^{2-}$ and $[Pt(mnt)_2]^{1-}$, mnt = $S_2C_2(CN)_2$ (Chart 2).[15]

(19) Amarasekera, J.; Rauchfuss, T. B.; Wilson, S. R. *J. Chem. Soc., Chem. Commun*. **1989**, 14.
(20) Venturelli, A.; Rauchfuss, T. B. *J. Am. Chem. Soc*. **1994**, *116*, 4824.
(21) Simon, G. L.; Dahl, L. F. *J. Am. Chem. Soc*. **1973**, *95*, 2164.
(22) Dobbs, D. A.; Bergman, R. G. *J. Am. Chem. Soc*. **1992**, *114*, 6908.
(23) (a) Simon, G. L.; Dahl, L. F. *J. Am. Chem. Soc*. **1973**, *95*, 2175. (b) Foust, A. S.; Dahl, L. F. *J. Am. Chem. Soc*. **1970**, *92*, 7337.
(24) (a) Harris, S. *Inorg. Chem*. **1987**, *26*, 4278 (b) Harris, S. *Polyhedron* **1989**, *8*, 2843. (c) Bahn, C. S.; Tan, A.; Harris, S. *Inorg. Chem*. **1998**, *37*, 2770. (d) Williams P. D.; Curtis, M. D. *Inorg. Chem*. **1986**, *25*, 4562. (e) Davies, C. E.; Green, J. C.; Kaltsoyannis, N.; MacDonald, M. A.; Qin, J.; Rauchfuss, T. B.; Redfern, C. M.; Stringer, G. H.; Woolhouse, M. G. *Inorg. Chem*. **1992**, *31*, 3779.
(25) McGrady, J. E. *J. Chem. Soc., Dalton Trans*. **1999**, 1393.

Chart 2. Schematic View of the Structures of $[(C_5H_5)_4Fe_4S_4]^{2+}$ Cations

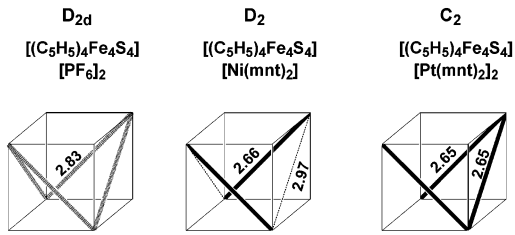

In the presence of $[Ni(mnt)_2]^{2-}$, the $[(C_5H_5)_4Fe_4S_4]^{2+}$ cluster adopts a D_2-symmetric structure with two short, two intermediate, and two long bonds. With a $[Pt(mnt)_2]^{1-}$ counterion, in contrast, two independent $[(C_5H_5)_4Fe_4S_4]^{2+}$ cations are found in the unit cell, both of which have C_2 symmetry. One has three almost identical short Fe−Fe bonds and is, therefore, isostructural with the ruthenium analogue, while the other is intermediate between the D_2- and C_2-symmetric structures. Thus, the three dications are structurally quite distinct from each other, and all three are different from that reported for $[(C_5H_5)_4Fe_4S_4][PF_6]_2$! No similar structural diversity has been noted for the ruthenium analogues, but a series of detailed variable temperature NMR studies[16] indicate that the dicationic cluster is fluxional in solution, suggesting that alternative cluster geometries are thermally accessible. These new structural results indicate that the $[(C_5H_5)_4Fe_4S_4]^{2+}$ cluster is remarkably plastic and can respond in very subtle ways to the steric demands of the counterion in the solid state. It is possible that this structural isomerism is simply a reflection of a very flat potential energy surface, in which case a continuum of different structural forms may exist, depending on the precise steric demands of the counterion. Similar observations have been made for the $Mo_2Cl_9^{3-}$ anion,[26,27] where the Mo−Mo separation varies systematically with the size of the cation. Alternatively, and more intriguingly, it is possible that two or more of the observed structures correspond to distinct minima on the potential energy surface of the isolated cluster. If the latter is the case, the system provides an example of the phenomenon of molecular bi- (or even tri-) stability that has attracted renewed attention in recent years.[28−30] In this contribution, we re-examine the electronic structure of the iron and ruthenium cubanes using density functional theory, with the aim of identifying the factors involved in determining their highly complex structural chemistry.

Computational Details

All calculations described in this paper were performed using the Amsterdam Density Functional (ADF) program, ADF2002.02.[31] A double-ζ Slater-type basis set, extended with a single polarization function, was used to describe the hydrogen, carbon, and sulfur atoms, while iron and ruthenium were modeled with a triple-ζ basis set. Electrons in orbitals up to and including 1s {C}, 2p{S}, 3p(Fe}, and 4p{Ru} were considered part of the core and treated in accordance with the frozen core approximation. The local density approximation was employed in all cases,[32] along with the local exchange-correlation potential of Vosko, Wilk, and Nusair[33] and gradient corrections to exchange and correlation proposed by Becke[34] and Perdew.[35] All structures were optimized using the gradient algorithm of Versluis and Ziegler.[36] In all optimizations, local 5-fold rotational symmetry was imposed for the C_5H_5 rings.

Table 2. Structures and Relative Energies of D_{2d}-Symmetric States $[(C_5H_5)_4Fe_4S_4]^{2+}$

electronic configuration	state	E_{rel}/eV	Fe–Fe/Å
$(1a_2)^2(3e)^0(2b_2)^0$	1^1A_1	+0.29	2.87 × 4, 3.20 × 2
$(1a_2)^1(3e)^0(2b_2)^1$	$^3B_1$	+0.05	2.86 × 4, 3.33 × 2
$(1a_2)^1(3e)^1(2b_2)^0$	**1^3E**	**0.00**	**2.85 × 4, 3.27 × 2**
	1^1E	+0.28	2.85 × 4, 3.27 × 2
$(1a_2)^0(3e)^2(2b_2)^0$	$^3A_2$	+0.20	2.85 × 4, 3.27 × 2
	2^1A_1, 3^1E	+0.43	2.85 × 4, 3.28 × 2
$(1a_2)^0(3e)^0(2b_2)^2$	3^1A_1	+0.25	2.81 × 4, 3.50 × 2
$[(C_5H_5)_4Fe_4S_4][PF_6]_2$			**2.834 × 4, 3.254 × 2**

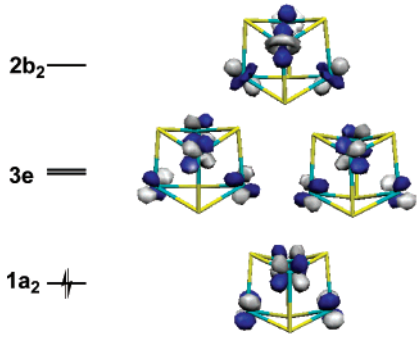

Figure 1. Molecular orbital array for the 1^1A_1 state of $[(C_5H_5)_4Fe_4S_4]^{2+}$ (C_5H_5 rings not shown).

Results and Discussion

Electronic Structure of $[(C_5H_5)_4Fe_4S_4]^{2+}$. According to the Dahl model described in the Introduction, the three vacant orbitals in the dication have b_2 and e symmetry, and a logical starting point for this investigation is therefore to establish whether this configuration gives rise to bond lengths similar to those reported for $[(C_5H_5)_4Fe_4S_4][PF_6]_2$. The optimized Fe−Fe bonds lengths of 2.87 and 3.20 Å in this state (1^1A_1, Table 2) represent a reasonable agreement with experiment, but the molecular orbital array shown in Figure 1 hints at greater complexity. The ordering of the three highest orbitals ($1a_2$, 3e, and $2b_2$) is as shown in Scheme 1, but the entire manifold spans only 0.02 eV (for comparison, the HOMO-1 (2e) lies almost 1 eV lower). This very narrow HOMO−LUMO gap suggests that the potential energy surface should feature a number of electronic states arising from the distribution of two electrons within this manifold, the Dahl configuration discussed above being only one of these.

(26) Stranger, R.; Grey, I. E.; Madsen, I. C.; Smith, P. W. *J. Solid State Chem.* **1987**, *69*, 162.
(27) (a) McGrady, J. E.; Stranger, R.; Lovell, T. *J. Phys. Chem. A* **1997**, *101*, 6265. (b) McGrady, J. E.; Stranger, R.; Lovell, T. *Inorg. Chem.* **1998**, *37*, 3802.
(28) McGrady, J. E. *Angew. Chem., Int. Ed.* **2000**, 3077.
(29) Clérac, R.; Cotton, F. A.; Daniels, L. M.; Dunbar, K. R.; Murillo, C. A.; Wang, X. *Inorg. Chem.* **2001**, *40*, 1256. (b) Clérac, R.; Cotton, F. A.; Daniels, L. M.; Dunbar, K. R.; Kirschbaum, K.; Murillo, C. A.; Pinkerton, A. A.; Schultz, A. J.; Wang, X. *J. Am. Chem. Soc.* **2000**, *122*, 6226. (c) Rohmer, M.-M.; Strich, A.; Bénard, M.; Malrieu, J.-P. *J. Am. Chem. Soc.* **2001**, *123*, 9126. (d) Benbellat, N.; Rohmer, M.-M.; Bénard, M. *Chem. Commun.* **2001**, 2368.
(30) Rohmer, M.-M.; Bénard, M. *Chem. Soc. Rev.* **2001**, 340.
(31) *ADF2001.01*; Theoretical Chemistry, Vrije Universiteit: Amsterdam. (a) Baerends, E. J.; Ellis, D. E.; Ros, P. *Chem. Phys.* **1973**, *2*, 42. (b) te Velde, G.; Baerends, E. J. *J. Comput. Phys.* **1992**, *99*, 84.
(32) Parr, R. G.; Yang, W. *Density Functional Theory of Atoms and Molecules*; Oxford University Press: New York, 1989.
(33) Vosko, S. H.; Wilk, L.; Nusair, M. *Can. J. Phys.* **1980**, *58*, 1200.
(34) Becke, A. D. *Phys. Rev. A* **1988**, *38*, 3098.
(35) Perdew, J. P. *Phys. Rev. B* **1986**, *33*, 8822.
(36) Versluis, L.; Ziegler, T. *J. Chem. Phys.* **1988**, *88*, 322.

A systematic survey reveals a total of eleven distinct states, all of which give rise, following structural optimization, to Aufbau configurations. [In most cases, the electronic configuration corresponds unambiguously to a single electronic state. The exception is the $(1a_2)^0(3e)^2(2b_2)^0$ configuration, which contributes to states of ^1E and $^1A_1$ symmetry.] Only seven of these bear relevance to the following discussion, and their structures and relative energies are summarized in Table 2. A full summary of all states, including structures and energies calculated using the LDA functional, is presented in the Supporting Information. The energetic reference point is arbitrary but is taken to be the 1^3E state.

A striking feature of the structural data summarized in Table 2 is the marked similarity in the optimized Fe−Fe bond lengths, all of which are in reasonable agreement with experiment (2.84−2.87 Å vs 2.834 Å). The one exception to this general rule is the 3^1A_1 state, where the highly distorted structure is a result of intramolecular electron transfer from sulfide to iron, leading to the formation of two S−S bonds. Although the presence of disulfide ligands in iron clusters is well established in the closely related bimetallic species $(C_5H_5)_2Fe_2S_4$ and $[(C_5H_5)_2Fe_2S_4]^{2+}$,[37] there is no experimental evidence to support their formation in $[(C_5H_5)_4Fe_4S_4]^{2+}$. It is not clear, therefore, whether this observation represents a realistic aspect of the excited-state chemistry of iron−sulfur cubanes or is simply an artifact of the calculation. In light of the rather high energy of the S−S bonded state, however, this issue does not impact significantly on our subsequent discussion.

The most important conclusion to emerge from Table 2 is that, while the Dahl configuration generates a structure consistent with experiment, so too do several alternative configurations. On structural grounds, therefore, there is little reason to favor any particular one as the most likely ground state. The calculated total energies, however, clearly indicate that a triplet state, 1^3E, is the most stable, lying some 0.29 eV below the Dahl configuration, 1^1A_1. The clear preference for a triplet ground state is to be expected in light of the near degeneracy of the HOMO and LUMO in Figure 1 but represents a marked departure from the closed-shell singlet proposed by Dahl. In this context, we note that magnetic susceptibility measurements indicate significant room-temperature paramagnetism.[38] We will return to this point following a discussion of the lower-symmetry isomers on the potential energy surface of the $[(C_5H_5)_4Fe_4S_4]^{2+}$ cation.

Reduction in Symmetry from D_{2d} to D_2. We noted in the previous section that the structure of the most stable D_{2d}-symmetric state, 1^3E, is very similar to the reported structure of the dication in $[(C_5H_5)_4Fe_4S_4][PF_6]_2$. The 1^3E state is, however, unstable with respect to a first-order Jahn−Teller distortion that removes the degeneracy of the 3e orbital, the two components of which are antibonding with respect to opposite edges of the tetrahedron. Their degeneracy can therefore be lifted by a rotation of one Fe_2 unit relative to the other about the principal axis (Figure 2), precisely the distortion required to drive the system toward the D_2-symmetric structure observed in $[(C_5H_5)_4Fe_4S_4][Ni(mnt)_2]$. The pseudo-degeneracy of the $\{1a_2, 3e, 2b_2\}$ manifold is partially lifted as a result, with the $3b_1$ and $2b_3$ orbitals significantly stabilized relative to the other two. The total energies and structures of the states arising from distribution of two electrons between these two low-lying orbitals are collected in Table 3, and the evolution of the state energies along the D_{2d} to D_2 coordinate is summarized in Figure 3. For consistency, the D_{2d}-symmetric 1^3E state is retained as the energetic reference point.

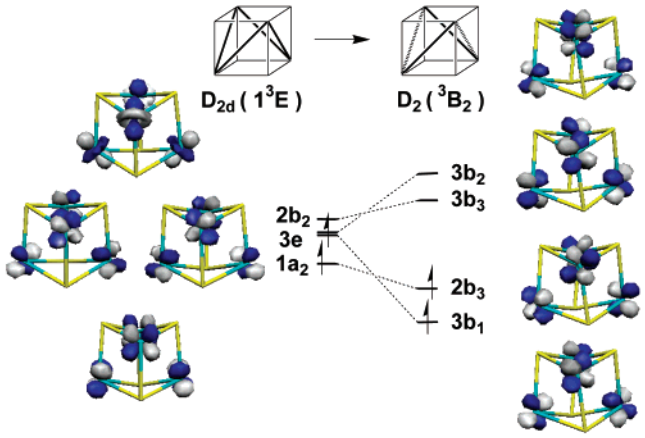

Figure 2. Evolution of frontier molecular orbitals on descent in symmetry from D_{2d} to D_2.

Table 3. Structures and Relative Energies of D_2-Symmetric States of $[(C_5H_5)_4Fe_4S_4]^{2+}$

electronic configuration	state	parent D_{2d} state	E_{rel}/eV	Fe–Fe/Å
$(3b_1)^0(2b_3)^2(3b_3)^0(3b_2)^0$	^1A	1^1A_1	+0.16	2.73 × 2, 3.00 × 2, 3.30 × 2
$(3b_1)^1(2b_3)^1(3b_3)^0(3b_2)^0$	**$^3B_2$**	**1^3E**	**−0.30**	**2.70 × 2, 3.02 × 2, 3.30 × 2**
$(3b_1)^1(2b_3)^1(3b_3)^0(3b_2)^0$	$^1B_2$	1^1E	+0.13	2.76 × 2, 2.93 × 2, 3.27 × 2
$(3b_1)^2(2b_3)^0(3b_3)^0(3b_2)^0$	^1A	2^1A_1, 3^1E	+0.07	2.68 × 2, 3.05 × 2, 3.31 × 2
$[(C_5H_5)_4Fe_4S_4][Ni(mnt)_2]$				**2.66 × 2, 2.97 × 2, 3.27 × 2**

The Jahn−Teller distortion splits the 1^3E state into a pair of D_2-symmetric states ($^3B_2$ and $^3B_1$) the former being stabilized by a clockwise rotation of the upper Fe_2 unit. The optimized structure of the $^3B_2$ state has Fe−Fe separations of 2.70, 3.02, and 3.30 Å, values that compare remarkably well with the crystallographic parameters of 2.66 Å, 2.97 Å, and 3.27 Å in $[(C_5H_5)_4Fe_4S_4][Ni(mnt)_2]$. Significantly, the total energies suggest that the driving force for this distortion is large, the $^3B_2$ state lying 0.30 eV below the parent 1^3E state. The corresponding open-shell singlet state, 1^1E, also has a single electron in the 3e orbital and is, therefore, effected to a similar degree, both structurally and energetically. The higher lying 3^1E state arises from the $(3e)^2(1a_2)^0(2b_2)^0$ configuration, and the double occupation of the 3e orbital provides a stronger driving force for the distortion. The resultant closed-shell singlet, 1^1A, is therefore stabilized to a greater extent (0.36 eV) relative to the D_{2d}-symmetric parent, and the structure shows a slightly greater distinction between the short and intermediate Fe−Fe bond

(37) (a) Weberg, R.; Haltiwanger, R. C.; Rakowski DuBois, M.; *Organometallics* **1985**, *4*, 1315. (b) Weberg, R.; Haltiwanger, R. C.; Rakowski DuBois, M. *New J. Chem.* **1988**, *12*, 361. (c) Brunner, H.; Janietz, N.; Meier, W.; Sergeson, G.; Watcher, J.; Zahn, T.; Ziegler, M. L. *Angew. Chem., Int. Ed. Engl.* **1985**, *24*, 1060. (d) Brunner, H.; Mertz, A.; Pfauntsch, J.; Serhadli, O.; Watcher. J.; Ziegler, M. L. *Inorg. Chem.* **1988**, *27*, 2055. (e) Ogino, H.; Tobita, H.; Inomata, S.; Shimoi, M. *J. Chem. Soc., Chem. Commun.* **1988**, 586. (f) Blasco, S.; Demachy, I.; Jean, Y.; Lledos, A. *New. J. Chem.* **2001**, *25*, 611.

(38) Wong, H.; Sedney, D.; Reiff, W. M.; Frankel, R. B.; Meyer, T.; Salmon, D. *Inorg. Chem.* **1978**, *17*, 194.

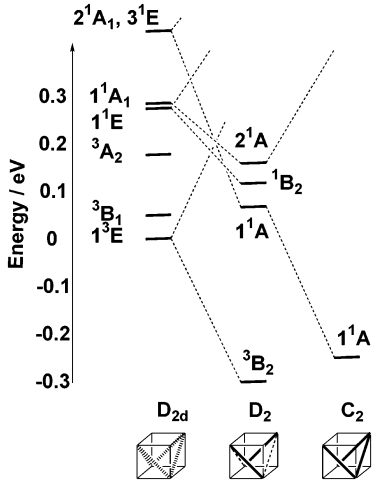

Figure 3. Evolution of selected electronic states of $[(C_5H_5)_4Fe_4S_4]^{2+}$ on descent in symmetry (D_{2d}−D_2−C_2).

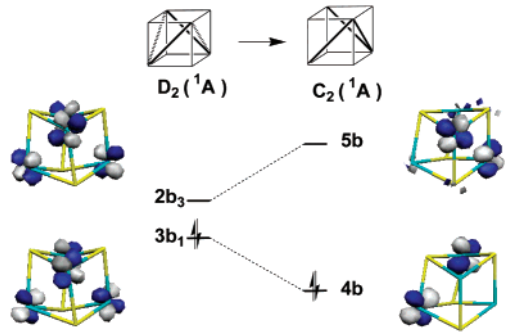

Figure 4. Evolution of frontier molecular orbitals on distortion from D_2 to C_2.

lengths (2.68 and 3.05 Å). In contrast, and as expected, the orbitally nondegenerate D_{2d}-symmetric states, $^3B_1$ and $^3A_2$, are stable with respect to a first-order Jahn−Teller distortion and revert back to the D_{2d}-symmetric structure when distorted. The D_{2d}-symmetric 1^1A_1 state *is*, however, stabilized by the reduction in symmetry from D_{2d} to D_2 (yielding 2^1A), despite the fact that it is also orbitally nondegenerate. This distortion can be traced to a second-order Jahn−Teller effect which allows the $1a_2$ and $2b_2$ orbitals of the D_{2d}-symmetric structure to mix upon reduction in symmetry, as both correlate with the b_3 representation of the D_2 point group.

Reduction in Symmetry from D_2 to C_2. On the D_2-symmetric potential energy surface, there is no remaining orbital degeneracy, so a first-order Jahn−Teller effect cannot explain any further distortion. Within the manifold of singlet states, however, a further second-order Jahn−Teller effect can operate to stabilize a C_2-symmetric distortion by allowing orbitals of b_1 and b_3 symmetry to mix (both correlate with the b representation of C_2). The in-phase combination of $3b_1$ and $2b_3$ affords an orbital that is antibonding across one edge, while the out-of-phase combination is antibonding across the other (Figure 4). The net result is a stabilization of a closed-shell singlet state (^1A) with optimized Fe−Fe separations (Table 4) of 2.71 Å, 2 × 2.72 Å, 2 × 3.32 Å, and 3.41 Å, in excellent agreement with values of 3 × 2.65 Å and 3 × 3.27 Å observed in one of the dications in $[(C_5H_5)_4Fe_4S_4][Pt(mnt)_2]_2$ (Table 4). The D_2−C_2 distortion coordinate is, however, relatively soft, and the somewhat less distorted structure observed in the second cation in $[(C_5H_5)_4Fe_4S_4][Pt(mnt)_2]_2$ lies only 0.05 eV above the C_2-symmetric ground state. It seems likely, therefore, that both cations in $[(C_5H_5)_4Fe_4S_4][Pt(mnt)_2]_2$ lie on the same potential energy surface (^1A), and crystal packing effects induce the variation in structure.

Table 4. Summary of the Structures and Relative Energies of Lowest Energy D_{2d}-, D_2-, and C_2-Symmetric States of $[(C_5H_5)_4Fe_4S_4]^{2+}$

symmetry	electronic configuration	state	E_{rel}/eV	Fe–Fe/Å
D_{2d}	$(1a_2)^1(3e)^1(2b_2)^0$	^3E	0.00	2.85 × 4, 3.27 × 2
D_2	$(3b_1)^1(2b_3)^1(3b_3)^0(3b_2)^0$	$^3B_2$	−0.30	2.70 × 2, 3.02 × 2, 3.30 × 2
C_2	$(4b)^2(5b)^0(6b)^0(6a)^0$	^1A	−0.26	2.71, 2.72 × 2, 3.32 × 2, 3.41

The structures and relative energies of the most stable states on the D_{2d}-, D_2- and C_2-symmetric potential energy surfaces of the $[(C_5H_5)_4Fe_4S_4]^{2+}$cation are collected in Table 4. The calculations clearly identify two states, $^3B_2$ (D_2) and ^1A (C_2), as the lowest lying on the global potential energy landscape of $[(C_5H_5)_4Fe_4S_4]^{2+}$, and crucially, both correspond closely to the structure of one of the known forms of the cation. The D_2-symmetric $^3B_2$ state is the most stable of the two, but the gap between this and the C_2-symmetric ^1A state is only 0.04 eV, making it impossible to make a definitive assignment of the global minimum for the gas-phase species (the order of the $^3B_2$ and ^1A states is in fact reversed at the LDA level of theory). Ultimately, however, it is not critical that we do so; the key point is that both the D_2- and C_2-symmetric isomers of $[(C_5H_5)_4Fe_4S_4]^{2+}$ correspond to distinct local minima on the gas-phase potential energy surface and the two lie close enough in energy for solid-state effects to perturb the balance between them.

What then of the D_{2d}-symmetric structure observed in $[(C_5H_5)_4Fe_4S_4][PF_6]_2$? Within the constraints of D_{2d} point symmetry, the most stable state is 1^3E, which certainly exhibits Fe−Fe similar bond lengths to those in the crystal, but the Jahn−Teller theorem tells us that this state cannot correspond to a minimum on the potential energy surface. It is possible that solid-state packing effects in $[(C_5H_5)_4Fe_4S_4][PF_6]_2$ could impose a D_{2d}-symmetric structure on the cation, but this seems rather unlikely given the strong driving force associated with the distortion. The location of a stable D_2-symmetric minimum, however, presents an alternative explanation for the apparent D_{2d} symmetry of the cation. An average of the two D_2-symmetric enantiomers, imposed either by a dynamic Jahn−Teller effect or by static disorder would result, on a crystallographic time scale, in effective D_{2d} symmetry. Significantly, the presence of a D_2- rather than D_{2d}-symmetric cation in $[(C_5H_5)_4Fe_4S_4][PF_6]_2$ is consistent with the other available physical data, most notably the equivalence of the iron centers observed in the Mössbauer spectrum and the nonzero room-temperature magnetic moment of the cluster. The pronounced reduction in this moment at low temperature,[38] is also consistent with the presence of a marginally more stable singlet state (of C_2 symmetry). It would be instructive to re-examine the crystal structure to determine whether the temperature dependence of the magnetic moment is indeed associated with a structural change.

Comparison with $[(C_5H_5)_4Ru_4S_4]^{2+}$. Optimized structural parameters and relative energies of the important D_{2d},- D_2-, and

Table 5. Summary of Structures and Relative Energies of All States of $[(C_5H_5)_4Ru_4S_4]^{2+}$

symmetry	electronic configuration	state	E_{rel}/eV	Ru–Ru/Å
D_{2d}	$(1a_2)^2(3e)^0(2b_2)^0$	1^1A_1	+0.31	3.06 × 4, 3.51 × 2
	$(1a_2)^1(3e)^0(2b_2)^1$	$^3B_1$	+0.22	3.06 × 4, 3.54 × 2
	$(1a_2)^1(3e)^1(2b_2)^0$	1^3E	0.00	3.04 × 4, 3.49 × 2
	$(1a_2)^0(3e)^2(2b_2)^0$	2^1A_1, 3^1E	+0.22	3.03 × 4, 3.54 × 2
		$^3A_2$	−0.14	3.02 × 4, 3.53 × 2
D_2	$(3b_1)^0(2b_3)^2(3b_3)^0(3b_2)^0$	2^1A	+0.11	2.95 × 2, 3.19 × 2, 3.55 × 2
	$(3b_1)^1(2b_3)^1(3b_3)^0(3b_2)^0$	$^3B_2$	−0.27	2.93 × 2, 3.18 × 2, 3.53 × 2
	$(3b_1)^2(2b_3)^0(3b_3)^0(3b_2)^0$	1^1A	−0.25	2.88 × 2, 3.21 × 2, 3.56 × 2
C_2	$(4b)^2(5b)^0(6b)^0(6a)^0$	^1A	−0.56	2.89, 2.92 × 2, 3.60 × 2, 3.68

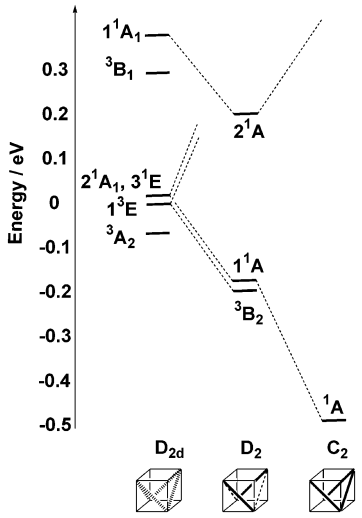

Figure 5. Evolution of selected electronic states of $[(C_5H_5)_4Ru_4S_4]^{2+}$ on descent in symmetry ($D_{2d}-D_2-C_2$).

C_2-symmetric states of the ruthenium cluster, $[(C_5H_5)_4Ru_4S_4]^{2+}$, are summarized in Table 5 and Figure 5. A comparison of the isoelectronic iron and ruthenium dications indicates that the general features of the potential energy surfaces are similar, but the more diffuse 4d orbitals in the latter introduce a number of subtle changes in the relative energies of the states. In the most symmetric (D_{2d}) case, the more effective overlap of the 4d orbitals leads to a selective destabilization of the $2b_2$ and $1a_2$ orbitals relative to 3e (Figure 1). The result is that, of the seven states summarized in Table 2, those that originate from the $(3e)^2(2b_2)^0(1a_2)^0$ configuration ($^3A_2$, ^3E, and 2^1A_1) are strongly stabilized relative to the others, leading to a $^3A_2$ ground state.

The same combination of first- and second-order Jahn−Teller distortions again stabilizes a D_2-symmetric triplet ($^3B_2$) and a C_2-symmetric singlet (^1A), but in marked contrast to the iron system, the latter is the more stable by 0.29 eV. The relative stability of the singlet manifold in comparison to the triplets is a clear reflection of both the greater covalent overlap between adjacent centers and the reduced electron−electron repulsions afforded by the 4d orbitals. The marked stabilization of the C_2-symmetric ^1A state enables us to assign it unambiguously as the global minimum in $[(C_5H_5)_4Ru_4S_4]^{2+}$, and its optimized structural parameters are indeed very similar to those in the only known crystal structure. The D_2-symmetric potential energy surface may, however, have a role to play in the fluxionality of the $[(CH_3C_5H_4)_4Ru_4S_4]^{2+}$ cation noted by Rauchfuss and coworkers. The experiment shows that all four ruthenium centers are interconverted by the fluxional process, with an activation free energy, $\Delta G^{\ddagger}$, of 52 kJ mol^{-1}, for which the authors proposed a D_{2d}-symmetric intermediate analogous to that reported for $[(C_5H_5)_4Fe_4S_4][PF_6]_2$. The calculated separation of 41 kJ mol^{-1} (0.42 eV) between the lowest states on the C_2- and D_{2d}-symmetric potential energy surfaces (^1A and $^3A_2$, respectively) is not inconsistent with the reported barrier, but the paramagnetic $^3A_2$ intermediate would lead to broadening of the NMR signal. The system, however, avoids the generation of paramagnetic intermediates by following a D_2-symmetric pathway, which also lies significantly lower in energy (0.31 eV, 30 kJ mol^{-1}). On this basis, the D_2-symmetric coordinate seems the more likely rearrangement pathway for the ruthenium cluster.

Summary

In this paper, we have used density functional theory to survey the potential energy surface of the dicationic clusters, $[(C_5H_5)_4Fe_4S_4]^{2+}$ and $[(C_5H_5)_4Ru_4S_4]^{2+}$. Taking the D_{2d}-symmetric structure as a reference point, we have been able to reduce the problem to the examination of all possible states arising from the distribution of two electrons within a manifold of four metal-based orbitals ($1a_2$, 3e, and $2b_2$). For the iron system, two structurally distinct states emerge with very similar total energies, a triplet with D_2 symmetry and a C_2-symmetric singlet. Their energetic proximity reflects the balance between covalent overlap (favoring the singlet) and electron−electron repulsions (favoring the triplet) in the rather contracted 3d orbitals. Both states represent local minima on the potential energy surface, and both correspond closely to the structure of the cluster in one of its known crystal forms. Thus, the delicate balance between covalent overlap and electron−electron repulsions leads directly to the rich structural chemistry of the iron clusters, as it allows the packing in the solid state to displace the system from one well-defined minimum to another. The calculations suggest that all D_{2d}-symmetric structures lie much higher in energy and, moreover, the most stable of them is orbitally degenerate and so cannot represent a minimum on the potential energy surface. On this basis, we propose that the apparent D_{2d}-symmetric structure of $[(C_5H_5)_4Fe_4S_4][PF_6]_2$ may result from disorder (dynamic or static) between the two enantiomeric forms of the D_2-symmetric cluster.

In the analogous ruthenium system, $[(C_5H_5)_4Ru_4S_4]^{2+}$, the more diffuse 4d orbitals enhance orbital overlap and at the same time reduce electron−electron repulsions. Both factors stabilize the C_2-symmetric closed-shell singlet over the D_2-symmetric triplet, as a result of which the former is unambiguously the ground state. The ruthenium system is therefore much less flexible than its iron analogue, and the only known structure corresponds closely to the optimized C_2-symmetric singlet. The D_2-symmetric potential energy surface does, however, present a viable low-energy pathway for the dynamic interchange of the Ru−Ru bonds observed in the variable temperature NMR spectra.

Acknowledgment. We thank the Engineering and Physical Sciences Research Council (U.K.) for financial support and the ORS for a studentship to S.Z.K.

Supporting Information Available: Relative energies and optimized structural parameters (BP86 and LDA functionals) for all states (D_{2d}, D_2, and C_2 symmetry) arising from double occupation of the $\{1a_2, 3e, 2b_2\}$ manifold for $[(C_5H_5)_4Fe_4S_4]^{2+}$ and $[(C_5H_5)_4Ru_4S_4]^{2+}$. Cartesian coordinates of optimized structures of all states. This material is available free of charge via the Internet at http://pubs.acs.org.

JA0353053